Supplemental material to this article can be found at:
http://molpharm.aspetjournals.org/content/suppl/2022/03/03/molpharm.121.000464.DC1
1521-0111/101/5/357–370$35.00
MOLECULAR PHARMACOLOGY
dx.doi.org/10.1124/molpharm.121.000464
Mol Pharmacol 101:357–370, May 2022

VU6036720: The First Potent and Selective In Vitro Inhibitor of Heteromeric Kir4.1/5.1 Inward Rectifier Potassium Channels[S]

Samantha J. McClenahan,[1] Caitlin N. Kent,[1] Sujay V. Kharade, Elena Isaeva, Jade C. Williams, Changho Han, Andrew Terker, Robert Gresham III, Roman M. Lazarenko, Emily L. Days, Ian M. Romaine, Joshua A. Bauer, Olivier Boutaud, Gary A. Sulikowski, Raymond Harris, C. David Weaver, Alexander Staruschenko, Craig W. Lindsley, and Jerod S. Denton

Departments of Anesthesiology (S.J.M., S.V.K., R.G., R.M.L., J.S.D.), Biochemistry (J.A.B.), Chemistry (C.N.K., J.C.W., I.M.R., C.D.W., G.A.S., C.W.L.), Pharmacology (E.L.D., C.D.W., C.W.L., C.H., O.B., J.S.D.), and Nephrology (A.T., R.H.), and Vanderbilt Institute of Chemical Biology (J.A.B., G.S., C.D.W., C.W.L., J.S.D.), Vanderbilt University, Nashville, Tennessee; Department of Cell Biology, Neurobiology and Anatomy, Medical College of Wisconsin, Milwaukee, Wisconsin (E.I.); and Department of Molecular Pharmacology and Physiology, University of South Florida, Tampa, Florida (A.S.)

Received November 18, 2021; accepted February 14, 2022

ABSTRACT

Heteromeric Kir4.1/Kir5.1 (*KCNJ10/KCNJ16*) inward rectifier potassium (Kir) channels play key roles in the brain and kidney, but pharmacological tools for probing their physiology and therapeutic potential have not been developed. Here, we report the discovery, in a high-throughput screening of 80,475 compounds, of the moderately potent and selective inhibitor VU0493690, which we selected for characterization and chemical optimization. VU0493690 concentration-dependently inhibits Kir4.1/5.1 with an IC_{50} of 0.96 μM and exhibits at least 10-fold selectivity over Kir4.1 and ten other Kir channels. Multidimensional chemical optimization of VU0493690 led to the development of VU6036720, the most potent (IC_{50} = 0.24 μM) and selective (>40-fold over Kir4.1) Kir4.1/5.1 inhibitor reported to date. Cell-attached patch single-channel recordings revealed that VU6036720 inhibits Kir4.1/5.1 activity through a reduction of channel open-state probability and single-channel current amplitude. Elevating extracellular potassium ion by 20 mM shifted the IC_{50} 6.8-fold, suggesting that VU6036720 is a pore blocker that binds in the ion-conduction pathway. Mutation of the "rectification controller" asparagine 161 to glutamate (N161E), which is equivalent to small-molecule binding sites in other Kir channels, led to a strong reduction of inhibition by VU6036720. Renal clearance studies in mice failed to show a diuretic response that would be consistent with inhibition of Kir4.1/5.1 in the renal tubule. Drug metabolism and pharmacokinetics profiling revealed that high VU6036720 clearance and plasma protein binding may prevent target engagement in vivo. In conclusion, VU6036720 represents the current state-of-the-art Kir4.1/5.1 inhibitor that should be useful for probing the functions of Kir4.1/5.1 in vitro and ex vivo.

SIGNIFICANCE STATEMENT

Heteromeric inward rectifier potassium (Kir) channels comprising Kir4.1 and Kir5.1 subunits play important roles in renal and neural physiology and may represent inhibitory drug targets for hypertension and edema. Herein, we employ high-throughput compound library screening, patch clamp electrophysiology, and medicinal chemistry to develop and characterize the first potent and specific in vitro inhibitor of Kir4.1/5.1, VU6036720, which provides proof-of-concept that drug-like inhibitors of this channel may be developed.

Introduction

Inward rectifier potassium (Kir) channels are tetrameric, membrane-spanning proteins that conduct potassium (K^+) ions down their electrochemical gradient to regulate cell excitability, hormone secretion, and transepithelial ion transport (Hibino et al., 2010; Welling, 2016). There are sixteen genes in the Kir channel family, and gain- or loss-of-function mutations in several of them are associated with human diseases. Sulfonylurea receptor (SUR) ligands that inhibit Kir6.2/SUR1 (K_{ATP}) channels in pancreatic beta cells stimulate insulin secretion and promote blood glucose homeostasis in patients with type II diabetes (Nichols, 2006). While other Kir channels are postulated to be drug targets for treating other diseases, a dearth of pharmacological tool compounds that are potent and selective enough to precisely modulate specific subtypes of Kir channels has been a critical barrier to rigorously validating these putative drug targets (Weaver and Denton, 2021).

Homotetrameric Kir4.1 and heterotetrameric Kir4.1/5.1 (Kir4.1 and Kir5.1 are encoded by *KCNJ10* and *KCNJ16,* respectively) channels are two subtypes of Kir channels

This work was funded in part by the National Institutes of Health [Grant R01-DK120821] (to J.S.D.), [Grant T32-NS007491] and [Grant F32-DK127679-01A1] (to S.J.M.), and [Grant R35-HL135749] (to A.S.),National Cancer Institute [Grant R50-CA211206] (to J.A.B.), and American Heart [Grant 1R25HL145330] (to R.G.). Tl+ flux experiments were performed in the Vanderbilt High-Throughput Screening Core Facility, which receives support from the Vanderbilt Institute of Chemical Biology and the Vanderbilt Ingram Cancer Center [P30 CA68485] The WaveFront Biosciences Panoptic kinetic imaging plate reader is housed and managed within the HTS Facility and was funded by National Institutes of Health Shared Instrumentation [Grant 1S10OD021734] (to C.W.L.). C.D.W. is an owner of WaveFront Biosciences and ION Biosciences manufacturers of the Panoptic and Thallos, respectively.

The authors declare that there are no actual or perceived conflicts of interest with the contents of this article.

[1]S.J.M. and C.N.K. contributed equally to this work.

dx.doi.org/10.1124/molpharm.121.000464.

[S] This article has supplemental material available at molpharm.aspetjournals.org.

expressed in the brain and kidney that may hold therapeutic potential for treating neurologic and cardiovascular diseases (Bockenhauer et al., 2009; Scholl et al., 2009; Reichold et al., 2010; Denton et al., 2013; Schlingmann et al., 2021). Kir4.1 forms functional K^+ channels on the plasma membrane when expressed alone, whereas Kir5.1 does not function on its own but can form heteromeric channels with Kir4.1 (Pessia et al., 1996).

Homomeric Kir4.1 is expressed primarily in brain astrocytes, where they help remove extracellular K^+ and glutamate released from actively firing neurons, in a process called spatial K^+ buffering (Kofuji et al., 2002; Djukic et al., 2007; Nwaobi et al., 2016). Changes in the expression levels of Kir4.1 and associated extracellular K^+ levels have been found in models of clinical depression (Cui et al., 2018; Frizzo and Ohno, 2021), ischemic stroke (Milton and Smith, 2018), and Huntington's disease (Tong et al., 2014; Jiang et al., 2016), suggesting a mechanistic link between Kir4.1 and these diseases. Kir4.1 channels have also been implicated in the behavioral and respiratory disturbances in Rett syndrome (Zhang et al., 2011; Kahanovitch et al., 2018), although their specific contributions in this polygenic disease are unclear.

Heteromeric Kir4.1/5.1 channels are the dominant channel subtype expressed in the kidney tubule (Welling, 2016; Manis et al., 2020; Weaver and Denton, 2021). Although they appear to be expressed throughout most of the nephron, Kir4.1/5.1 channels play especially important roles in regulating sodium, chloride and K^+ balance by the distal convoluted tubule (DCT) and cortical collecting duct (Zhang et al., 2014; Terker et al., 2015; Su and Wang, 2016; Cuevas et al., 2017; Su et al., 2019). The importance of Kir4.1 and Kir4.1/5.1 channels in humans was definitively established with the discovery that loss-of-function mutations in *KCNJ10* cause epilepsy, ataxia, sensorineural deafness, tubulopathy/seizures, sensorineural deafness, ataxia, mental disability, tubulopathy syndrome, an autosomal recessive disorder characterized by epilepsy, ataxia, sensorineural deafness, intellectual disability, and renal salt wasting (Bockenhauer et al., 2009;Scholl et al., 2009; Reichold et al., 2010). Similarly, recent studies revealed that mutations in *KCNJ16* are associated with hypokalemia, salt wasting, disturbed acid-base homeostasis, and sensorineural deafness (Schlingmann et al., 2021; Webb et al., 2021).

Kir4.1 and Kir4.1/5.1 channels differ significantly in their functional and regulatory properties, as well as their sensitivity to small-molecule inhibitors. For example, heteromeric Kir4.1/5.1 channels have a larger unitary conductance, lower open-state probability, and greater sensitivity to changes in intracellular pH than homomeric Kir4.1 (Lagrutta et al., 1996; Tucker et al., 2000; Pessia et al., 2001). The molecular pharmacology of the two channels is still very rudimentary; however, homomeric Kir4.1 is known to be inhibited by the serotonin reuptake inhibitors fluoxetine and nortriptyline, and the tricyclic antidepressant amitriptyline (Ohno et al., 2007; Furutani et al., 2009). Unfortunately, these compounds are relatively weak inhibitors (i.e., IC_{50}s in the tens of micromoles) and exhibit broad inhibitory activity toward several other members of the Kir channel family. Chloroquine (Marmolejo-Murillo et al., 2017b) and pentamidine (Arechiga-Figueroa et al., 2017) also inhibit Kir4.1, but their usefulness as in vivo tool compounds is limited. We recently reported the discovery of a moderately potent (IC_{50}=1 μM), in vivo–active Kir4.1 inhibitor that is ninefold selective over Kir4.1/5.1 and greater than 30-fold selective over Kir1.1, Kir2.1, and Kir2.2, demonstrating that the development of tool compounds capable of discriminating between homomeric Kir4.1 and heteromeric Kir4.1/5.1 channels and other members of the Kir family is feasible (Kharade et al., 2018). Here, we report the successful development and detailed characterization of the first potent and selective Kir4.1/5.1 channel inhibitor: VU6036720.

Methods

Molecular Biology and Human Embryonic Kidney (HEK)-293–Kir4.1/5.1 Cell Line Generation. Expression plasmids carrying the cDNA sequence of human Kir4.1 or Kir5.1 were purchased from Origene Technologies. To ensure that both channel subunits are expressed in transfected cells, the cDNAs were subcloned into different multiple cloning sites of the bicistronic vector pBudCE4.1 (Invitrogen). The hKir4.1 cDNA was subcloned downstream of the cytomegalovirus promoter, whereas the hKir5.1 cDNA was subcloned downstream of the elongation factor 1α promoter using gene synthesis methods by GenScript. The Kir5.1-asparagine 151-to-glutamate mutation was created using the QuickChange mutagenesis kit (Agilent Technologies) according to the manufacturer's instructions. The correct cDNA sequences were verified with DNA sequencing.

HEK-293T cells were transfected using Lipofectamine LTX reagent according to the manufacturer's protocol and then placed under antibiotic selection using 700 ug/ml of zeocin. Single clones were isolated from stably transfected polyclonal cells using limiting dilution methods, expanded, and then screened for robust Kir4.1/5.1-mediated thallium (Tl^+) flux using the methods described below. Stably transfected monoclonal T-Rex- HEK-293 cell lines expressing Kir1.1, Kir2.2, Kir2.2, Kir2.3, Kir4.1, Kir4.2, Kir6.1/ SUR2B, Kir6.2/ SUR1, Kir7.1-M125R, or Kv11.1 (human EAG-related gene) were generated and cultured as described previously (Lewis et al., 2009; Bhave et al., 2011; Raphemot et al., 2011; Raphemot et al., 2013; Swale et al., 2016). HEK-293 cells expressing human EAG-related genes were constructed as described (Kaufmann et al., 2013).

Quantitative Tl^+ Flux Assay of Kir4.1/5.1 Activity. High-throughput Tl^+ flux fluorescence-based assay was performed in the Vanderbilt High-Throughput Screening Center essentially as described previously (Kharade et al., 2018). Briefly, HEK-293–Kir4.1/5.1 cells were cultured overnight in Dulbecco's modified Eagle's medium containing 10% FBS at 37°C and 5% CO_2 in 384-well plates. The following day, the cells were incubated with dye-loading assay buffer (Hank's

ABBREVIATIONS: CI, confidence interval; CL_{hep}, predicted hepatic clearance; CRC, concentration-response curve; DCT, distal convoluted tubule; DMPK, drug metabolism pharmacokinetics; f_u, fraction unbound; HCTZ, hydrochlorothiazide; HEK, human embryonic kidney; HTS, high-throughput screening; K^+, potassium ion; Kir, inward rectifier potassium; LC/MS/MS, liquid chromatography tandem mass spectrometry; NCC, sodium-chloride symporter; PK, pharmacokinetic; SAR, structure-activity relationship; SUR, sulfonylurea receptor; $T_{1/2}$, half-life; TFA, trifluoroacetic acid; Tl^+, thallium ion.

balanced salt solutions, 20 mM of HEPES, pH 7.3) containing 0.01% (w/v) Pluronic F-127 (Life Technologies) and 1.2 μM of Tl^+-reporting dye Thallos Gold (Dutter et al., 2018) (or "Pluronic") or Brilliant Thallium (Ion Biosciences, Austin, TX) in ambient conditions for 1 hour with 20 ul/well of assay buffer, washing before and after dye using Hanks' balanced salt solution/20 mM HEPES (assay buffer). Media and buffer exchange were performed on an ELx405 TS plate washer (BioTek, Winooski, VT). Dye-loaded cells were then transferred to a Panoptic Kinetic Imaging Plate Reader (Wavefront Bioscience, Franklin, TN) to collect live measurements at 1 Hz (482/35 nm excitation and 536/40 nm emission Brilliant Thallium; 517/20 nM excitation and 580/60 nm emissions Thallos Gold) during simultaneous 384-well pipetting of 10-μM small molecules (0.1% DMSO) or control (100 μM of fluoxetine). Compounds were incubated for 4 minutes before the addition of Tl^+ stimulus buffer (125 mM of $NaHCO_3$, 1.8 mM of $CaSO_4$, 1 mM of $MgSO_4$, 5 mM of glucose, 1.2 mM of Tl_2SO_4, and 10 mM of HEPES, pH 7.4 titrated with NaOH). Live measurements were collected 10 seconds before the addition of compounds to 2 minutes after Tl^+ stimulus addition.

For identified hits in the primary screen and structure-activity relationship libraries, compounds were tested at concentrations to obtain 10-point, threefold dilution concentration-response curves. Data acquisition and analysis were performed using Waveguide (VU-HTS center) and Microsoft Excel. IC_{50} values were determined by fitting the Hill equation using variable-slope nonlinear regression analyses performed with GraphPad Prism version 5.01 (GraphPad Software, San Diego, CA).

Whole-Cell Patch Clamp Electrophysiology. HEK-293T cells were transfected with wild-type (WT) pBudCE4.1-Kir4.1/5.1 or combinations of pcDNA5-Kir4.1 and pcDNA5-Kir5.1 with pcDNA3.1-EGFP transfection marker) using Lipofectamine LTX reagent according to the manufacturer's instructions. The cells were dissociated the following day and plated on poly-L-lysine–coated coverslips and allowed to recover for at least 1 hour in a 37°C 5% CO_2/95% air incubator before beginning experiments. Patch electrodes (2–3 mega Ohm) were filled with an intracellular solution containing 135 mM of KCl, 2 mM of $MgCl_2$, 1 mM of EGTA, 10 mM of HEPES-free acid, and 2 mM of Na_2ATP (Roche Diagnostics, Risch-Rotkreuz, Switzerland), pH 7.3, titrated with KOH and 275 mOsmol/kg of water. The standard bath solution contained 135 mM of NaCl, 5 mM of KCl, 2 mM of $CaCl_2$, 1 mM of $MgCl_2$, 5 mM of glucose, and 10 mM of HEPES free acid, pH 7.4 titrated with NaOH. Macroscopic currents were recorded under whole-cell voltage-clamp conditions using an Axopatch 200B Amplifier (Molecular Devices, Sunnyvale, CA). Cells were voltage-clamped at a holding potential of -75 mV and stepped every 5 seconds to -120 mV for 200 milliseconds before ramping to +120 mV at a rate of 1.2 mV/ms. Data were collected at 5 kHz and filtered at 1 kHz. Data acquisition and analysis were performed using the pClamp 9.2 software suite (Molecular Devices). Pharmacology experiments were terminated by applying 2 mM of barium (Ba^{2+}) chloride to block the heterologously expressed Kir currents and measure residual leak current. Cells exhibiting <90% block by Ba^{2+} were excluded from the analysis. The mean current amplitude recorded over five successive steps to -120 mV in cells at a single concentration was expressed as the mean ± S.D. IC_{50} values were determined by fitting the Hill equation to concentration-response curves (CRCs) using variable-slope nonlinear regression analyses. All the analyses were performed with GraphPad Prism version 5.01 (GraphPad Software).

Single-Channel Electrophysiology Recordings. Chinese hamster ovary (CHO) cells were used for single-channel recordings because they express very little endogenous K^+ channel activity that could interfere with these recordings. Cells were maintained under standard culture conditions (F12K, 10% FBS, 100 U/ml of penicillin-streptomycin, 37°C, 5% CO_2), and transfected with pIRES-Kir4.1, pBudCE4.1-Kir4.1/Kir5.1, or pBudCE4.1-Kir4.1/5.1-N161E with eGFP plasmid DNA using the Polyfect reagent (Qiagen, Valencia, CA) according to the manufacturer's protocol. Patch-clamp recordings of inwardly rectifying K^+ currents were carried out 24–48 hours following transfection. Single-channel Kir4.1 and Kir4.1/Kir5.1 activity were performed in cell-attach voltage-clamp configuration using an Axopatch 200B amplifier (Molecular Devices) and Digidata 1440A analog-to-digital converter (Molecular Devices). Recordings were made using extracellular solution (in mM): 150 NaCl, 5 KCl, 1 $CaCl_2$, 2 $MgCl_2$, 5 glucose, and 10 HEPES, pH 7.35, titrated with NaOH. Patch electrodes were filled with a solution of the following composition (in mM): 100 NaCl, 50 KCl, 2 $MgCl_2$, and 10 HEPES, pH 7.35, titrated with NaOH and had resistances from 8 to 10 MΩ. Currents were low-pass filtered at 0.3 kHz with an eight-pole Bessel filter (Warner Instruments, Hamden, CT). Channel activity was assessed using Clampfit 10.6 software (Molecular Devices). Statistical analysis was performed using two-sided paired *t* test or one-way ANOVA with Bonferroni multiple comparison test, as appropriate, with statistical significance defined at $P < 0.0167$ and 0.05, respectively.

Renal Clearance Studies. Ten-week-old male C57Bl/6 mice were used for urine collection studies. Five mice were orally gavaged with vehicle (10% Tween 80 in PBS) and five with VU6036720 at a dose of 30 or 100 mg/kg prior to a four-hour urine collection in metabolic cages. One week later, the vehicle group was gavaged with VU6036720 at 30 mg/kg, and the group that received VU6036720 was gavaged with vehicle prior to another four-hour urine collection. Seven of the mice underwent a third gavage treatment with VU6036720 at 100 mg/kg two weeks later prior to another four-hour urine collection. Three mice that had previously received either vehicle or VU6036720 received the diuretic hydrochlorothiazide (HCTZ) as a positive control.

General Chemistry Methods. All NMR spectra were recorded on a 400 MHz AMX Bruker NMR spectrometer. ^1H and ^{13}C chemical shifts are reported in δ values in ppm downfield with the deuterated solvent as the internal standard. Data are reported as follows: chemical shift, multiplicity (s = singlet, d = doublet, t = triplet, q = quartet, b = broad, m = multiplet), coupling constant (Hz), and integration. Low resolution mass spectra were obtained on an Agilent 6120 or 6150 with electrospray ionization source. Method A: Mass spectrometry parameters were as follows: fragmentor: 70; capillary voltage: 3000 V; nebulizer pressure: 30 psig; drying gas flow: 13 L/min; drying gas temperature: 350°C. Samples were introduced via an Agilent 1290 UHPLC comprised of a G4220A binary pump, G4226A automatic liquid sampler, G1316C thermostatted column compartment, and G4212A diode array detector with ultra-low-dispersion flow cell. UV absorption was generally observed at 215 nm

and 254 nm with a 4 nm bandwidth. Column: Waters Acquity BEH C18, 1.0 × 50 mm, 1.7 um. Gradient conditions: 5 to 95% CH_3CN in H_2O (0.1% trifluoroacetic acid; TFA) over 1.4 minutes, hold at 95% CH_3CN for 0.1 minutes, 0.5 ml/min, 55°C. Method B: Mass spectrometry parameters were as follows: fragmentor: 100, capillary voltage: 3000 V, nebulizer pressure: 40 psig, drying gas flow: 11 L/min, drying gas temperature: 350°C. Samples were introduced via an Agilent 1200 HPLC comprised of a degasser, G1312A binary pump, G1367B high-performance automatic liquid sampler, G1316A thermostatted column compartment, G1315D diode array detector, and a Varian 380 evaporative light scattering detector (if applicable). UV absorption was generally observed at 215 nm and 254 nm with a 4-nm bandwidth. Column: Thermo Accucore C18, 2.1 × 30 mm, 2.6 um. Gradient conditions: 7 to 95% CH_3CN in H_2O (0.1% TFA) over 1.6 minutes, hold at 95% CH_3CN for 0.35 minutes, 1.5 ml/min, 45°C. High-resolution mass spectra were obtained on an Agilent 6540 UHD quadrupole time-of-flight with electrospray ionization source. Mass spectrometry were as follows: fragmentor: 150, capillary voltage: 3500 V, nebulizer pressure: 60 psig, drying gas flow: 13 L/min, drying gas temperature: 275°C. Samples were introduced via an Agilent 1200 UHPLC comprised of a G4220A binary pump, G4226A automatic liquid sampler, G1316C thermostatted column compartment, and G4212A diode array detector with ultra-low-dispersion flow cell. UV absorption was observed at 215 nm and 254 nm with a 4-nm bandwidth. Column: Agilent Zorbax Extend C18, 1.8 μm, 2.1 × 50 mm. Gradient conditions: 5 to 95% CH_3CN in H_2O (0.1% formic acid) over 1 minute, hold at 95% CH_3CN for 0.1 minutes, 0.5 ml/min, 40°C. Optical specific rotations were obtained using a JASCO P-2000 Digital Polarimeter equipped with a tungsten-halogen lamp (WI), 589 nm wavelength, photomultiplier tube (1P28-01) detector and CG2-100 Cylindrical glass cell, 2.5ø x 100 mm. For compounds that were purified on a Gilson preparative reversed-phase high-performance liquid chromatography system comprised of a 333 aqueous pump with solvent-selection valve, 334 organic pump, GX271 or GX-281 liquid hander, two column switching valves, and a 155 UV detector. UV wavelength for fraction collection was user-defined, with absorbance at 254 nm always monitored. Method 1: Phenomenex Axia-packed Luna C18, 30 × 50 mm, 5-μm column. Mobile phase: CH_3CN in H_2O (0.1% TFA). Gradient conditions: 0.75-minute equilibration, followed by user defined gradient (starting organic percentage, ending organic percentage, duration), hold at 95% CH3CN in H_2O (0.1% TFA) for 1 minute, 50 ml/min, 23°C. Method 2: Phenomenex Axiapacked Gemini C18, 50 × 250 mm, 10-um column. Mobile phase: CH_3CN in H_2O (0.1% TFA). Gradient conditions: 7-minute equilibration, followed by user defined gradient (starting organic percentage, ending organic percentage, duration), hold at 95% CH_3CN in H_2O (0.1% TFA) for 7 minutes, 120 ml/min, 23°C. Chiral separation was performed on a Thar (Waters) Investigator SFC Column: Chiral Technologies CHIRALPAK IF, 4.6 × 250 mm, 5-μm column. Gradient conditions: 20 to 50% isopropyl alcohol in CO_2 over 7 minutes, hold at 50% CO_2 for 1 minute. Flow rate: 3.5 ml/min. Column temperature: 40°C. System backpressure: 100 bar. Solvents for extraction, washing, and chromatography were high-performance liquid chromatography grade. All reagents were purchased from Aldrich Chemical Co. and were used without purification. All compounds described in the structure-activity relationship (SAR) tables were >95% pure by liquid chromatography mass spectrometry (214 nm, 254 nM and evaporative light scattering detector) as well as ^1H NMR.

Initially, small quantities of VU0493690 were purchased from Life Chemicals (Niagara-on-the-Lake ON), and larger quantities were prepared following a variation of the experimental procedure below for the synthesis of VU6036720.

Chemical Synthesis. See Supplemental Methods.

Hepatic Microsomal Intrinsic Clearance. Human, rat, and mouse hepatic microsomes (0.5 mg/ml) and 1 μM of test compound were incubated in 100 mM of K^+ phosphate pH 7.4 buffer with 3 mM of $MgCl_2$ at 37°C with constant shaking. After a 5-minute preincubation, the reaction was initiated by addition of nicotinamide adenine dinucleotide phosphate (1 mM). At selected time intervals (0, 3, 7, 15, 25, and 45 minutes), aliquots were taken and subsequently placed into a 96-well plate containing cold acetonitrile with internal standard (50 nM carbamazepine). Plates were then centrifuged at 3000 RCF (4°C) for 10 minutes, and the supernatant was transferred to a separate 96-well plate and diluted 1:1 with water for liquid chromatography tandem mass spectrometry (LC/MS/MS) analysis. The in vitro half-life ($t_{1/2}$, min), intrinsic clearance (ml/min/kg), and subsequent predicted hepatic clearance (CL_{hep}, ml/min/kg) were determined using Eqs. 1 – 3:

$$T_{1/2} = \frac{Ln(2)}{k} \quad (1)$$

Eq. 1. Determination of half-life. k represents the slope from linear regression analysis of the natural log percent remaining of test compound as a function of incubation time.

$$CL_{int} = \frac{0.693}{in\ vitro\ T_{1/2}} \ x\ \frac{1\ mL\ incubation}{0.5\ mg\ microsomes} \ x\ \frac{45\ mg\ microsomes}{1\ gram\ liver} \ x\ \frac{20^a\ gram\ liver}{kg\ body\ wt} \quad (2)$$

Eq. 2. Determination of intrinsic clearance. [a]scale-up factors (gm liver/kg body weight) of 20 (human), 45 (rat), and 87.5 (mouse) were used in this calculation (scaling factors were derived from (Lin et al., 1996).

$$CL_{hep} = \frac{Q_h * CL_{int}}{Q_h + CL_{int}} \quad (3)$$

Eq. 3. Determination of predicted hepatic clearance. Q_h represents hepatic blood flow (ml/min/kg): 21 for human, 70 for rat, and 90 for mouse.

Plasma-Protein and Brain-Homogenate Binding. The protein binding of each compound was determined in plasma via equilibrium dialysis employing rapid equilibrium dialysis plates (ThermoFisher Scientific, Rochester, NY). Plasma was added to the 96-well plate containing test compound and mixed thoroughly for a final concentration of 5 μM. Subsequently, an aliquot of the plasma-compound mixture was transferred to the *cis* chamber (red) of the rapid equilibrium dialysis plate, with a phosphate buffer (25 mM, pH 7.4) in the *trans* chamber. The rapid equilibrium dialysis plate was sealed and incubated for 6 hours at 37°C with shaking (120 rpm). At completion, aliquots from each chamber were transferred to a new 96-well plate and were diluted 1:1 with either plasma (*trans*) or buffer (*cis*) and transferred to a new 96-well plate, at which time ice-cold acetonitrile containing

internal standard (50 nM carbamazepine) (3 volumes) was added to extract the matrices. The plate was centrifuged (3000 RCF, 10 minutes) and supernatants transferred and diluted 1:1 (supernatant: water) into a new 96-well plate, which was then sealed in preparation for LC/MS/MS analysis. Each compound was assayed in triplicate within the same 96-well plate.

A similar approach was used to determine the degree of brain homogenate binding, which employed the same methodology and procedure with the following modifications: 1) a final compound concentration of 1 μM was used, and 2) naïve rat brains were homogenized in Dulbecco's phosphate-buffered saline (1:3 composition of brain: Dulbecco's phosphate-buffered saline, w/w) using a Mini-Bead Beater machine to obtain brain homogenate, which was then treated in the same manner as the plasma samples in the previously described plasma protein binding assay. Fraction unbound for both plasma and brain samples was determined using Eq. 4.

$$f_u = \frac{Conc_{buffer}}{Conc_{plasma}} \quad (4)$$

Eq. 4. Determination of fraction unbound in plasma. The diluted fraction unbound (f_u) 2 in brain was calculated in the same manner by using brain homogenate rather than plasma. Undiluted fraction unbound for the brain was calculated using Eq. 5.

$$f_u = \frac{1/4}{\left\{\left(\frac{1}{fu2}\right) - 1\right\} + 1/4} \quad (5)$$

Eq. 5. Determination of fraction unbound in brain. F_u2 represents the diluted fraction unbound.

Rat IV PBL Plasma Brain Level Cassette. Male Sprague-Dawley rats (n = 2) weighing around 300 g were purchased from Harlon Laboratories (Indianapolis, IN) and implanted with catheters in the carotid artery and jugular vein. The cannulated animals were acclimated to their surroundings for approximately one week before dosing and provided food and water ad libitum. IV cassette pharmacokinetic (PK) experiments in rats were carried out according to methods described previously (Bridges et al., 2014). Briefly, a cassette of compounds (n = 4–5 compounds/cassette) was formulated from 10-mM solutions of compounds in DMSO. To reduce the absolute volume of DMSO that was administered, the compounds were combined and diluted with ethanol and PEG 400 to achieve a final concentration of 0.4–0.5 mg/ml for each compound (2 mg/ml total) administered in each cassette. The final dosing solutions consisted of approximately 10% ethanol, 40% PEG400, and 50% DMSO (v/v). Each cassette dose was administered IV via the jugular vein to two dual-cannulated (carotid artery and jugular vein) adult male Sprague–Dawley rats, each weighing between 250 and 350 g (Harlan, Indianapolis, IN) for a final dose of 0.2–0.25 mg/kg per compound. Whole blood collections via the carotid artery were performed at 0.033, 0.117, 0.25, 0.5, 1, 2, 4, 7, and 24 hours post dose and plasma samples prepared for bioanalysis. For tissue distribution studies in cassette format, brain dissection and blood collections via the carotid artery were performed at 0.25 hours post dose. Blood samples were collected into chilled, EDTA-fortified tubes, centrifuged for 10 minutes at 3000 rpm (4°C), and the resulting plasma was aliquoted into 96-well plates for LC/MS/MS analysis. The brain samples were rinsed in PBS, snap frozen and stored at -80°C. Prior to LC/MS/MS analysis, whole brain samples were thawed to room temperature and subjected to mechanical homogenation in 3 ml of 70:30 isopropyl alcohol:water employing a Mini-Beadbeater and 1.0 mm Zirconia/Silica Beads (BioSpec Products) for 3 minutes and centrifuged at 3500 g for 5 minutes. Five microliters of the supernatant was diluted in 15 µl of blank plasma for quantification of the analytes. Discrete IV PK experiments in rats (n = 2) were carried out analogously at a dose of 1.0 mg/kg in 10% EtOH, 50% PEG 400, and 40% saline, while discrete PO PK experiments in rats (n = 2) were carried out using a 3 mg/kg dose of compounds in a fine microsuspension in 30% Captisol in H_2O via oral gavage to fasted animals. Whole blood collections via the carotid artery were performed at 0.117, 0.25, 0.5, 1, 2, 4, 7, and 24 hours post dose. Plasma samples were centrifuged at 3500 g for 5 minutes. A standard curve was generated by diluting the analyte DMSO stocks with blank plasma to obtain a final concentration of 10,000 ng/ml, followed by a serial dilution down to 0.5 ng/ml. Quality controls were generated by a serial dilution of the 5000 ng/ml standard curve solution in blank plasma to obtain 3 concentrations of 500, 50, and 5 ng/ml. Twenty microliters of brain diluted in plasma, plasma, blank plasma, standard curve, and quality control samples were loaded in a V-bottom 96-well plate. One hundred twenty microliters of acetonitrile containing 50 nM of carbamazepine (internal standard) was added in each well, and the plate was centrifuged at 3500 g for 5 minutes. Sixty microliters of the supernatant of each well (protein free) was transferred to a new 96-well plate containing 60 ul of water. The plates were sealed for analysis by LC-MS/MS.

LC/MS/MS Bioanalysis of Samples. Plasma and brain tissue samples originating from in vivo studies were analyzed by electrospray ionization using an AB Sciex Q-TRAP 5500 (Foster City, CA) that was coupled to a Shimadzu LC-20AD pump (Columbia, MD) and a Leap Technologies CTC PAL auto-sampler (Carrboro, NC). Analytes were separated by gradient elution using a C18 column (3 × 50 mm, 3 mm; Fortis Technologies, Ltd., Cheshire, UK) that was thermostated at 40°C. High-performance liquid chromatography mobile phase A was 0.1% formic acid in water (pH unadjusted); mobile phase B was 0.1% formic acid in acetonitrile (pH unadjusted). A 10% B gradient was held for 0.2 minutes and was linearly increased to 90% B over 0.8 minutes, with an isocratic hold for 0.5 minutes, before transitioning to 10% B over 0.05 minutes. The column was re-equilibrated (1 minute) before the next sample injection. The total run time was 2.55 minutes, and the HPLC flow rate was 0.5 ml/min. The source temperature was set at 500°C, and mass spectral analyses were performed using a turbo ion spray source in positive ionization mode (5.0-kV spray voltage) and using multiple-reaction monitoring of transitions specific for each analyte. All data were analyzed using AB Sciex Analyst 1.5.1 software. The lower limits of quantitation were determined at 1.0 ng/ml in plasma and in brain homogenates.

Mouse IV and PO PK Studies. Ten-week-old male C57Bl/6 mice were used for the pharmacokinetic studies performed at Frontage Laboratories, Inc. (Exton, PA). Three mice were administered intravenously with VU6036720 in ethanol: PEG400: saline (10:70:20 v/v/v) at 1 mg/kg. Three mice were orally gavaged with VU6036720 in 10% Tween 80 in water at 10 or 100 mg/kg. Blood samples were collected from all mice at 8 different time points post-dose. The

concentration of VU6036720 in blood was quantified by LC/MS/MS as described above.

The IV PK experiment was used to determine clearance, volume of distribution and half-life. The PO experiments were used to determine exposure and oral bioavailability. PK parameters of VU6036720 were calculated using Phoenix WinNonlin software (version 8.1).

Results

Electrophysiological Characterization of HEK-293–Kir4.1/5.1 Cells. Kir4.1/5.1 channels were expressed from the bicistronic vector, pBudCE4.1, to ensure that both subunits are expressed at approximately equal levels in stably transfected cells. In comparison with non-transfected HEK-293 cells, which exhibited only small-amplitude, outwardly rectifying endogenous currents (Fig. 1A), stably transfected cells exhibit robust, inwardly rectifying whole-cell currents that are characteristic of Kir4.1/5.1 currents (Fig. 1B)(Tucker et al., 2000). As expected, the currents were fully inhibited by Ba^{2+} (Fig. 1, C–D) and reversed near the Nernst equilibrium potential for K^+, indicating that the dominant whole-cell current is carried by heterologously expressed Kir4.1/5.1.

Development and Validation of the Kir4.1/5.1 Tl^+ Flux Assay for High-Throughput Screening (HTS). Heteromeric Kir4.1/5.1 channels exhibit functional, regulatory, and pharmacological properties that are distinct from homomeric Kir4.1 (Tucker et al., 2000; Pessia et al., 2001). To confirm that our HEK-293–Kir4.1/5.1 cell line expresses primarily heteromeric channels, we compared the pharmacological properties of the HEK-293–Kir4.1/5.1 cell line to those of an HEK-293 cell line that stably expresses homomeric Kir4.1 (Kharade et al., 2018).

The experiments were performed using quantitative Tl^+ flux assays that use the intracellular fluorescent dye, Thallos-AM, to report the inward movement of the K^+ congener Tl^+ through Kir4.1/5.1 or Kir4.1 channels overexpressed in the HEK-293 cell membrane. The assays were performed in 384-well plates so that experiments on Kir4.1/5.1 and Kir4.1 could be performed in parallel. As shown in Fig. 2A, Tl^+ addition to a well containing HEK-293–Kir4.1/5.1 cells caused a robust increase in fluorescence emission as Tl^+ moved inwardly through the expressed channels and excited the dye. Pre-addition of the control inhibitor fluoxetine (50 μM) led to a strong reduction in the Tl^+-induced fluorescence increase. Parallel experiments performed on stably transfected HEK-293–Kir4.1/5.1 and HEK-293–Kir4.1 cells showed that the channels are pharmacologically distinct. We constructed concentration-response curves (CRCs) for both cell lines using the known Kir4.1 blockers fluoxetine (Ohno et al., 2007), amitriptyline (Su et al., 2007), and VU0134992 (Kharade et al., 2018). Of the three compounds tested, fluoxetine and amitriptyline were the most potent inhibitors of Kir4.1/5.1, exhibiting IC_{50} values of 20.1 μM (confidence interval (CI): 18.6–21.3 μM) and 20.8 μM (CI:19.2–22.5 μM), respectively (Fig. 2, B and D). Fluoxetine and amitriptyline inhibited homomeric Kir4.1 channels with IC_{50} values of 48.6 μM (CI: 37.2–102.6 μM) and 81.7 μM (CI: very wide). As we reported previously (Kharade et al., 2018), VU0134992 exhibits approximately ninefold selectivity for Kir4.1 (IC_{50}=6.1 μM; CI: 5.5–6.6 μM) over Kir4.1/5.1 (IC_{50}=51.7 μM; CI: 42.0–77.0 μM) (Fig. 2C). It is notable that our previous studies were performed using a

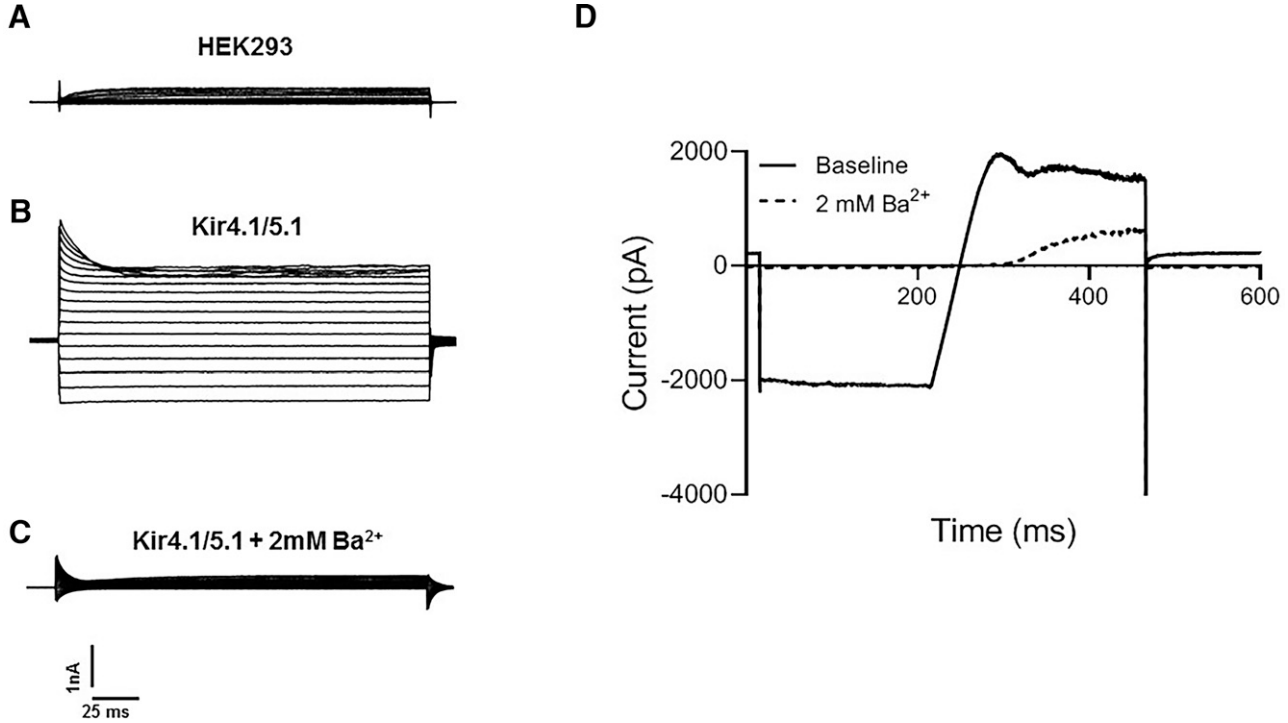

Fig. 1. Electrophysiological properties of human embryonic kidney-293-inward rectifier potassium (Kir) 4.1/5.1 cells. (A) Exemplar whole-cell currents recorded from non-transfected human embryonic kidney-293 cells evoked with 200-millisecond steps between -120 mV and 120 mV from a holding potential of -75 mV. (B) Currents evoked using the same voltage clamp protocol but from stably transfected monoclonal inward rectifier potassium 4.1/5.1 cells. (C) Residual currents following bath application of 2 mM of barium. (D) Currents evoked using a step-ramp protocol used for concentration-response experiments before and after block with barium. See Methods for details.

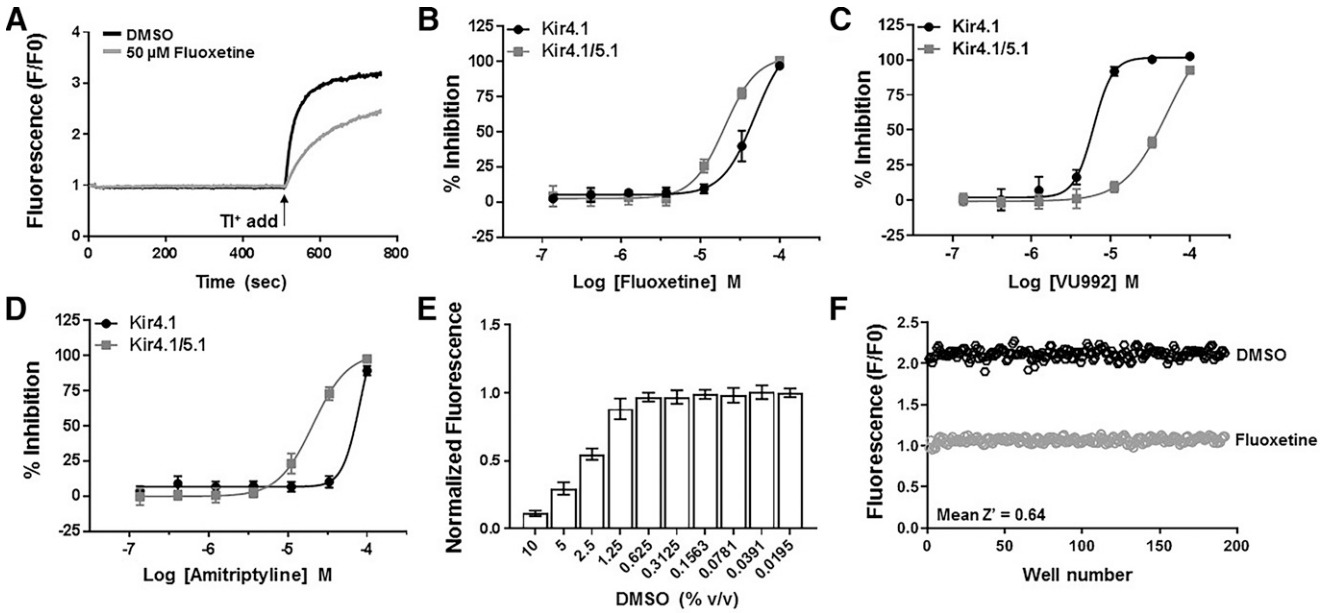

Fig. 2. Development and validation of inward rectifier potassium (Kir) 4.1/5.1 Tl^+ flux assay for high-throughput screening. (A) Representative thallium ion (Tl^+) flux experiment in which Thallos fluorescence is recorded from human embryonic kidney (HEK)-293-Kir4.1/5.1 cells plated a 384-well plate, treated with either 0.1% v/v DMSO (solvent control) or 50 μM of fluoxetine (control blocker) before adding Tl^+ stimulus buffer to wells (arrow). The fluorescence increase is inhibited by the Kir4.1/5.1 blocker fluoxetine. concentration-response curves against HEK-293–Kir4.1/5.1 cells (gray, square symbols) or HEK-293–Kir4.1 cells (black, circle symbols) using (B) fluoxetine (Kir4.1/5.1 IC_{50} = 20.1 μM; Kir4.1 IC_{50} = 48.6 μM), (C) VU992 (Kir4.1/5.1 IC_{50} =51.7 μM; Kir4.1 IC_{50} = 6.1 μM), or (D) amitriptyline (Kir4.1/5.1 IC_{50} = 20.8 μM; Kir4.1 IC_{50} = 81.7 μM). Data are means ± S.E.M. from triplicate experiments performed on two separate days. (E) DMSO tolerance curve. HEK-293–Kir4.1/5.1 cells were incubated with the indicated concentrations of DMSO for 10 minutes before initiating Tl^+ flux experiments. Note that Tl^+ flux is unaffected at concentrations up to 1.25% v/v, indicating that screening and other experiments in which DMSO is <0.3% v/v are unaffected by the solvent. Data are means ± S.E.M. from triplicate experiments performed on two separate days. (F) Representative scatter plot of "checkerboard" experiments in which alternative wells of a 384-well plate are treated with either DMSO (solvent control) or 50 μM of fluoxetine (control Kir4.1/5.1 blocker) for 10 minutes before initiating Tl^+ flux. Note the clear separation between the two cell/well populations. This experiment was performed in triplicate on three separate days, yielding a mean Z' value of 0.64.

concatemeric channel construct in which Kir4.1 and Kir5.1 were physically connected by a linker and thereby forced to assemble into heteromeric channels. The excellent agreement between the two datasets strongly suggests the channels expressed in the HEK-293–Kir4.1/5.1 cell line are likely heteromeric Kir4.1/5.1 channels.

We validated the suitability of the Kir4.1/5.1 Tl^+ flux assay for library screening by evaluating its tolerance to the small-molecule solvent DMSO, as well as its well-to-well, plate-to-plate, and day-to-day uniformity. DMSO tolerance was tested by incubating Kir4.1/5.1 cells in increasing concentrations of DMSO and then subjected to Tl^+ flux analysis. As shown in Fig. 2E, Kir4.1/5.1-mediated Tl^+ flux was insensitive to DMSO at concentrations up to 1.25% v/v, above which Tl^+ flux dropped off dose-dependently. This tolerance range is important because screening is done at a DMSO concentration of 0.1% v/v, which does not directly interfere with Kir4.1/5.1 channel activity. The uniformity of the assay was assessed by performing checkerboard assays in which alternative wells of a 384-well plate are treated with either DMSO (0.1% v/v) or fluoxetine (control inhibitor). The scatter plot in Fig. 2F shows normalized fluorescence (see Methods) data recorded from wells of a single 384-well plate treated with either DMSO or 50 μM of fluoxetine. The experiment was repeated using three different plates on three separate days. The mean ± SD Z' calculated from these experiments was 0.64 ± 0.08, indicating that the assay is sufficiently uniform and reproducible to enable high-confidence hit picking in a primary screen.

Discovery and Characterization of VU0493690. We screened 80,475 compounds from the Vanderbilt Discovery Collection (Life Chemicals, Woodbridge, CT, USA) for novel inhibitors and activators of Kir4.1/5.1. The mean ± SD Z' plate statistic for the 253-plate screen was 0.714 ± 0.04, indicating robust assay performance. A summary of the number of inhibitors (427), weak inhibitors (719), activators (145), weak activators (946), and negative compounds (the remainder of compounds) is illustrated in Fig. 3A. Hits were retested in duplicate and counter-screened against parental (non-transfected) HEK-293 cells resulting in 157 activators and 291 inhibitors that were retest positive and dependent on Kir4.1/5.1 expression. Concentration-response experiments were performed on the top 90 most potent inhibitor showing the largest decrease in Tl^+ flux at 10 μM by evaluating their potency in 10-point CRCs. VU0493690 (Fig. 3B) was one of the first moderately potent inhibitors discovered early in the screening and was therefore re-synthesized to confirm its structure and activity. In Tl^+ flux assays, VU0493690 concentration-dependently inhibited Kir4.1/5.1 activity with an IC_{50} of 3.2 μM (CI: 2.7–3.8 μM), which is approximately sixfold more potent than fluoxetine (IC_{50} = 19.5 μM; CI: 12.1–31.3 μM) (Fig. 3C). In patch clamp experiments, VU0493690 inhibited Kir4.1/5.1 currents completely at 10 μM (Fig. 3D) and concentration-dependently at -120 mV with an IC_{50} of 0.96 μM (CI: 0.25–1.6 μM) (Fig. 3E). At a concentration of 10 μM, VU0493690 inhibited homomeric Kir4.1 current at -120 mV by only 7.8 ± 1.9% (n = 5; data not shown), affording greater than 10-fold selectivity for Kir4.1/5.1 over Kir4.1.

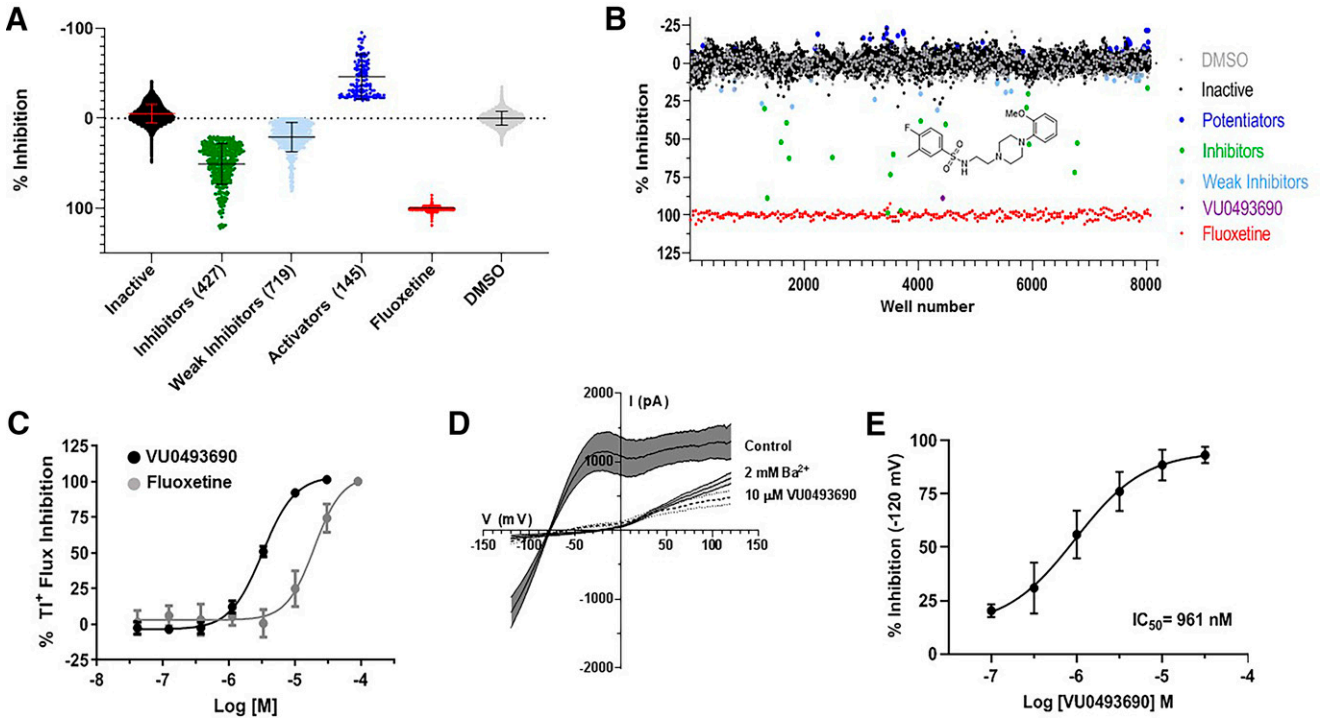

Fig. 3. Discovery and characterization of inward rectifier potassium (Kir) 4.1/5.1 inhibitor VU0493690. (A) Human embryonic kidney-293-Kir4.1/5.1 cells plated in 384-well plates were treated with 0.1% v/v DMSO (solvent control), 100 µM of fluoxetine (control blocker), or test compounds at a nominal concentration of 10 µM for 10 minutes before initiating thallium ion (Tl^+) flux. Test compounds were assigned either inactive (black), potentiators (dark blue), weak hits (light blue), or inhibitors (green) based on their effect on Tl^+ flux relative to vehicle controls. Hit categories were defined per 384-well plate as exceeding 3 standard deviations of the mean Tl^+ response in both slope and amplitude. These values are plotted as a percentage of maximal inhibition defined by fluoxetine as the control. Weaker hits only exceeded in either slope or amplitude (weak potentiators not shown). (B) Scatter plot showing the discovery of VU043690 (purple circle) among several thousand other test compounds. The chemical structure of VU043690 is shown in the inset. (C) Comparison of VU043690 (black) and fluoxetine (gray) concentration-response curves in Kir4.1/5.1 in Tl^+ flux assays. Data are means ± S.E.M. from triplicate experiments performed on two separate days. IC_{50} values derived from logistical fits to the data are 3.2 µM and 19.5 µM for VU043690 and fluoxetine, respectively. (D) Confirmation of VU0493690 activity against Kir4.1/5.1 in whole-cell patch-clamp orthogonal assays. Data are means ± S.E.M. (n = 4–5) where S.E.M. is indicated in shaded area. Two millimolar barium was used as a control blocker. (E) VU043690 concentration-response curve in whole-cell patch clamp experiments. Data are means ± SD (n = 4–5).

The selectivity of VU0493690 for Kir4.1/5.1 versus eleven other members of the Kir channel family was evaluated in concentration-response experiments using established Tl^+ flux assays (Raphemot et al., 2011; Raphemot et al., 2014; Swale et al., 2016; Kharade et al., 2018). At concentrations ranging between 0.3 nM and 30 µM, VU0493690 is greater than 30-fold selective for Kir4.1/5.1 over homomeric Kir4.1 channels, Kir1.1, Kir2.1, Kir2.2, Kir2.3, Kir4.2, Kir6.2/SUR1, Kir6.1/SUR2b, and Kir7.1 (Table 1). However, weak activity toward Kir3.1/3.2 (13% inhibition at 30 µM) and Kir3.1/3.4 (18% inhibition at 30 µM), and Kir6.1/SUR2b (19% inhibition at 30 µM) were observed. We also evaluated the activity of VU0493690 against the cardiac K^+ channel, human EAG-related gene (Kv11.1), in which VU0493690 had greater than 10-fold selectivity (Table 1).

VU0493690 SAR and Development of VU6036720. While VU0493690 was the most potent and selective Kir4.1/5.1 inhibitor reported to date, a more potent tool was required for proof of concept and target validation studies in pre-clinical animal models. A multi-dimensional optimization campaign, as depicted in Fig. 4, sought to identify productive regions of SAR to improve target potency and drug metabolism pharmacokinetic (DMPK) profile. Piperazine replacements, such as [3.3.0] and other spirocyclic congeners proved inactive. A wide range of alternatively substituted aryl and heteroaryl sulfonamides were prepared and evaluated, and only a 3-chloro-4-fluoro congener **3** proved as potent (Kir4.1/5.1 Tl^+ IC_{50} = 3.5 μM) as VU0493690. Maintaining this moiety and surveying alternative aryl groups on the distal piperazine led to the discovery of a 2-cyanophenyl derivative **4** with a slight improvement in potency (Kir4.1/5.1 Tl^+ IC_{50} = 2.6 μM). With these SAR findings in hand, we then evaluated the addition of chiral methyl groups to the piperazine core of **4**, in an effort to further improve on target potency. The chemistry to arrive as these analogs is shown in Supplemental Fig. 1, with the route to VU6036720 exemplified. Starting from commercial (S)-5, a Buchwald coupling affords N-Ar piperazine **6** in 89% yield. Boc-deprotection proceeds in quantitative yield delivering **7**, which is then alkylated to provide **8**. Another deprotection gives **9**, and a reaction with a sulfonyl chloride delivers the final compound **10** (VU6036720). Interestingly, the SAR proved to be highly regio-and enantiospecific. As highlighted in Fig. 5, 2-methyl substituted piperazines **10** and **11** showed clear enantiospecific activity, with the (*S*)-enantiomer **10** being more potent (Kir4.1/5.1 Tl^+ IC_{50} = 0.73 μM) than the HTS hit, while the (*R*)-enantiomer **11** was inactive. Installation of chiral methyl groups in the 3-position, as with **12** and **13**, was unproductive, leading to weak or inactive analogs. At concentrations ranging between 0.3 nM to 30 µM, VU6036720 remained greater than 30-fold selective for Kir4.1/5.1 over homomeric Kir4.1 channels, Kir1.1, Kir2.1, Kir2.2, Kir2.3, Kir4.2, Kir6.2/SUR1, Kir6.1/SUR2b, and Kir7.1, similar to

TABLE 1
Selectivity of VU6036720 over members of the inward rectifier potassium channel family and data are mean IC_{50} values (in μM) derived from concentration response curves performed in triplicate. Inactive compounds are those that inhibited the indicated channel by less than 50% at 30 μM and exhibited no trend in curve-fitting analyses. Numbers in parentheses indicate the maximal percent inhibition at 30 μM. Fluoxetine or the indicated compounds were used as control inhibitors.

Channel	VU0493690	VU6036720	Fluoxetine	Special Controls
Kir4.1/5.1	3.2 (100%)	2.2 (100%)	11.2	18.9 (VU0134992)
Kir4.1	Inactive	Inactive	32.5 (32%)	8.02 (VU0134992)
Kir4.2	Inactive	Inactive	39.5	3.4 (VU0134992)
Kir1.1	Inactive	Inactive	35.5 (18)	0.243 (VU591)
Kir7.1	Inactive	>30 (33%)	NA	6.4 (ML 418)
Kir2.1	Inactive	Inactive	>30 (5%)	7.3 (ML133)
Kir2.2	Inactive	Inactive	>30 (1%)	21.5 (ML133)
Kir2.3	Inactive	>30 (17%)	26.6	9.6 (ML133)
Kir3.1/3.2	>30 (13%)	>30 (9%)	4.32	8.24 (SCH23390)
Kir3.1/3.4	>30 (18%)	>30 (8%)	7.8	6 (SCH23390)
Kir6.2/SUR1	Inactive	Inactive	>30	0.008 (Glibenclamide)
Kir6.1/SUR2b	>30 (19%)	>30 (54%)	8.01	0.024 (Glibenclamide)
Kv11.1	11.4 (61%)	6.4 (92%)	5.1	3.9 (Quinidine)

that of VU0493690 (Table 1). A detailed SAR optimization description is outside of the scope of this manuscript and will be reported in due course.

Effect of VU6036720 on Kir4.1/5.1 Single Channel Properties. Cell-attached patch recordings were performed to determine how VU6036720 inhibits Kir4.1/5.1 at the single-channel level. Fig. 6A shows a representative recording before (a) and after (b) bath application of 10 μM of VU6036720. The same recordings at an expanded time scale are shown in Fig. 6B. As shown in the summary data (Fig. 6C) from 8 independent recordings, 10 μM VU6036720 led to a significant ($P < 0.05$) decrease in N, P_o, and single-channel amplitude.

VU6036720 Blocks the Kir4.1/5.1 Channel Pore Near Asparagine 161. Several structurally diverse small-molecule Kir channel inhibitors block the pore through interactions with residues that comprise the so-called "rectification controller" located below the selectivity filter (reviewed in (Swale et al., 2014) and (Weaver and Denton, 2021)). A common feature of these pore blockers is their tendency to

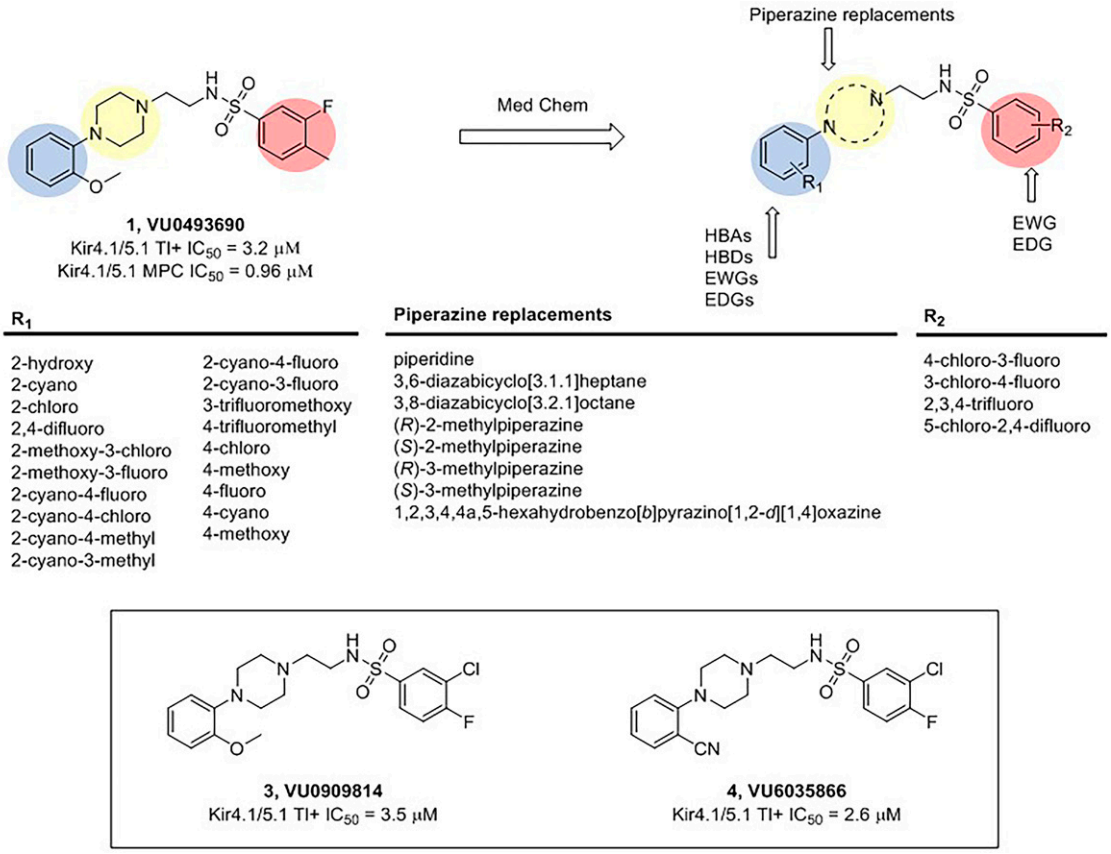

Fig. 4. Multi-dimensional optimization plan for 1, VU0493690, and initial productive structure-activity relationships affording 3 and 4. HBAs, hydrogen bond acceptors; HBDs, hydrogen bond donors; EWGs, electron withdrawing groups; EDGs, electron donating groups.

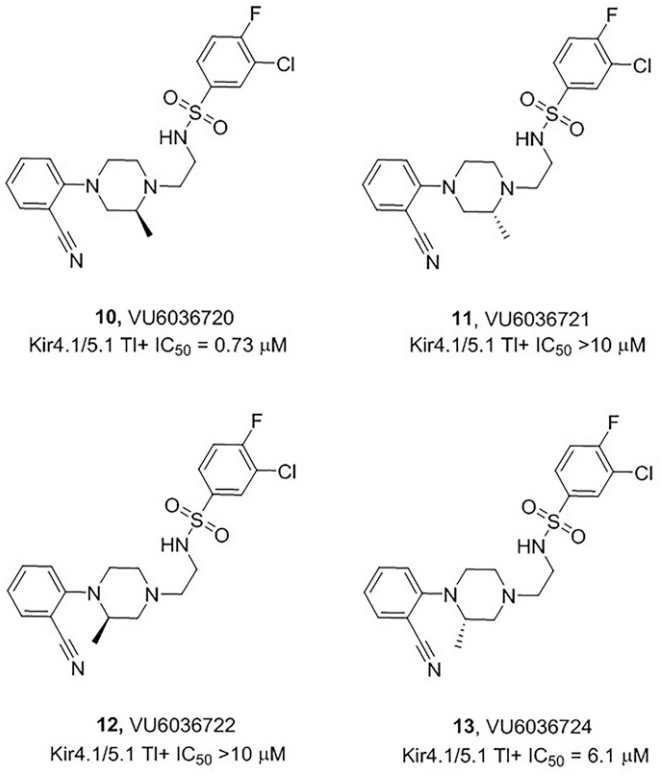

Fig. 5. Structure-activity relationship of regio-and enantiopure methyl piperazine analogs 10–13.

exhibit K^+-dependent "knockoff", whereby elevation of extracellular K^+ weakens binding in the pore. As a first step toward testing if VU6036720 is a Kir4.1/5.1 pore blocker, we constructed a CRC for VU6036720 in the presence of 25 mM of bath K^+. As shown in Fig. 7A, the elevation of extracellular K^+ right-shifted the CRC and increased the VU6036720 IC_{50} of VU6036720 to 1.6 μM (25K, gray curve), which represents a 6.8-fold shift from that recorded in 5 mM of bath K^+ (black curve).

The rectification controller of Kir4.1 is glutamate 158 (E158), and mutation of this residue reduces channel block by fluoxetine, nortriptyline, pentamidine, quinacrine, and VU0134992 (Furutani et al., 2009; Arechiga-Figueroa et al., 2017;Marmolejo-Murillo et al., 2017a; Kharade et al., 2018). Alignment of the Kir4.1 and Kir5.1 (Fig. 7B, bottom panel) amino acid sequences reveals that the equivalent residue in Kir5.1 is asparagine 161 (N161). The location of N161 is mapped onto the Kir2.2 model in Fig. 7B (top panels). Given the importance of this pore region in the small-molecule block, we tested if mutation of Kir5.1-N161 to glutamate (Kir5.1-N161E) reduces the sensitivity of Kir4.1/5.1 channels to VU6036720. A potential caveat of this experiment is that the Kir5.1-N161E mutation could prevent the formation of heteromeric channels, leading to the expression of homomeric Kir4.1 channels, which are markedly less sensitive to VU6036720 (Table 1). We, therefore, compared the single-channel properties of Kir4.1/5.1-N161E with those of wild-type Kir4.1/5.1 and Kir4.1. Representative current recordings for the three channel subtypes are shown in Fig. 7C, whereas the mean ± SD IV plots and single-channel conductance data are summarized in Fig. 7, D and E, respectively. As expected from published literature, the single-channel conductance of Kir4.1 is significantly ($P < 0.001$) smaller than that of wild-type Kir4.1/5.1. Importantly, the single-channel conductance of Kir4.1/5.1-N161E is not different from its wild-type counterpart, indicating that the N161E mutation does not prevent heteromultimerization with Kir4.1. We, therefore, used this construct to test the role of N161 in the mechanism of VU6036720 action. As shown in Fig. 7F, mutation of Kir5.1-N161E led to a striking reduction in VU6036720 block (filled triangles), which was similar to that of homomeric Kir4.1 (filled circles). In these experiments, the IC_{50} for Kir4.1 was much greater than 10 μM, affording greater than 40-fold selectivity of VU6036720 for Kir4.1/5.1 over Kir4.1.

VU6036720 Does Not Induce Diuresis in vivo. Having developed the most potent and selective Kir4.1/5.1 inhibitor reported to date, we tested if VU6036720 could induce diuresis by inhibiting renal Kir4.1/5.1 channel activity in mice. The animals were gavaged with either vehicle control, 30 mg/kg of VU6036720, 100 mg/kg of VU6036720, or the diuretic HCTZ (25 mg/kg) and placed in metabolic cages for 4 hours to collect urine. In contrast to HCTZ, which induced a significant ($P < 0.05$) increase in urine output, neither 30 mg/kg nor 100 mg/kg of VU6036720 stimulated urine production (Supplemental Fig. 2).

DMPK Properties of VU6036720. We profiled VU6036720 in a battery of in vitro and in vivo DMPK assays in an effort to understand its inability to induce urine production in vivo (Table 2). VU6036720 was compliant with Lipinski rules and had a favorable xLogP of 2.78. In addition, VU6036720 had modest fraction unbound across species (f_u human = 0.013; f_u rat = 0.009 and f_u mouse = 0.019) and similar brain homogenate binding (f_u brain rat = 0.007 and f_u brain mouse = 0.020). Unfortunately, the compound displayed high predicted hepatic clearance across species (CL_{hep} human – 20.3 ml/min/kg; CL_{hep} rat – 68.9 ml/min/kg; CL_{hep} mouse – 89.4 ml/min/kg). In vivo IV/PO PK experiment confirmed that VU6036720 was highly metabolized in mouse (plasma clearance mouse – 124 ml/min/kg; 137.7% QH) and had very low oral bioavailability (1.3%) (Table 2). Based on these data, metabolite identification studies are underway to identify metabolic hot spots to improve the pharmacokinetic profile.

Discussion

Here we describe the development of a small-molecule inhibitor, VU6036720, with unprecedented potency and selectivity for heteromeric Kir4.1/5.1 over homomeric Kir4.1. With an IC_{50} in Tl^+ flux assays of approximately 3 μM (Table 1), VU6036720 is approximately seven times more potent at inhibiting Kir4.1/5.1 than fluoxetine (IC_{50} = 20 μM; Fig. 2B) and amitriptyline (IC_{50} = 20 μM; Fig. 2D). The actual IC_{50} for VU6036720 from gold-standard whole-cell voltage clamp experiments is approximately 240 nM, making it greater than 40-fold selective over Kir4.1 ($IC_{50} > 10$ μM). Thus, VU6036720 represents the current state-of-the-art in Kir4.1/5.1 channel inhibitors.

The screening assay was developed using a bicistronic vector that enables approximately equal expression of both Kir4.1 and Kir5.1 subunits in transfected cells, which should promote the formation of predominantly heterotetrameric channels for study. Several lines of evidence suggest that this is the case. Tl^+ flux experiments clearly showed that channels

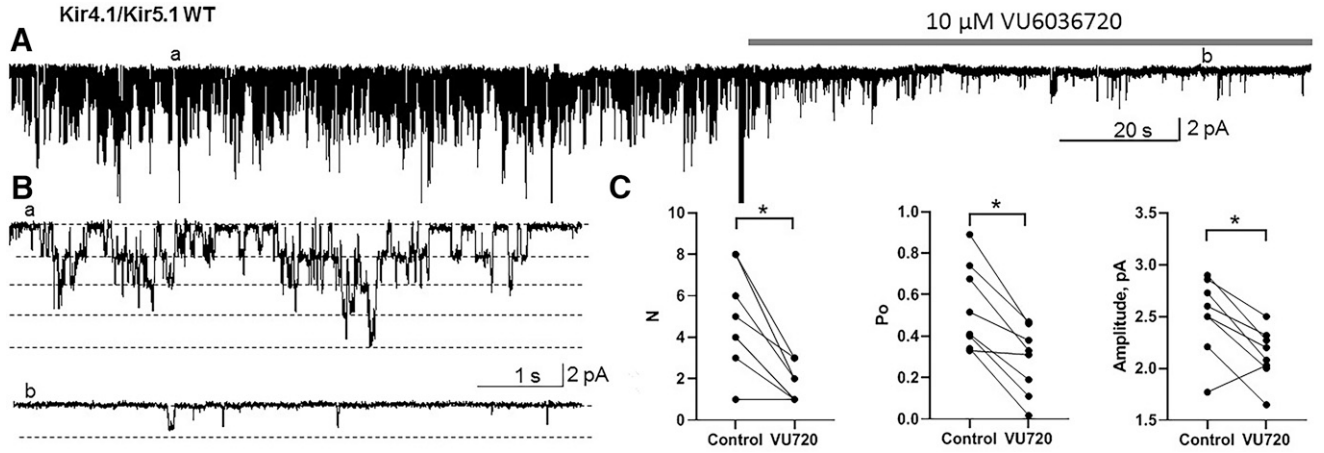

Fig. 6. Effects of VU6036720 on inward rectifier potassium 4.1/5.1 single-channel properties. (A) Cell-attached patch single-channel recordings of inward rectifier potassium 4.1/5.1 channel activity before (a) and after (b) bath application of 10 μM VU6036720. (B) Channel activity from (a) and (b) shown at higher temporal resolution. (C) Summary of single-channel data showing significant (*$P < 0.0167$) effects of VU6036720 on N, P_o, and amplitude.

in HEK-293–Kir4.1/5.1 cells are pharmacologically distinct from those expressed in HEK-293–Kir4.1 cells. For example, concentration-response-experiments using the Kir4.1-preferring inhibitor VU0134992 revealed a ninefold selectivity for Kir4.1 over Kir4.1/5.1, which is the same selectivity window we reported from patch clamp recordings comparing homomeric Kir4.1 channels and a Kir4.1/5.1 concatemer where the two subunits are physically coupled together to ensure heteromultimerization (Kharade et al., 2018). Pharmacological separation between the two cell lines was also observed for

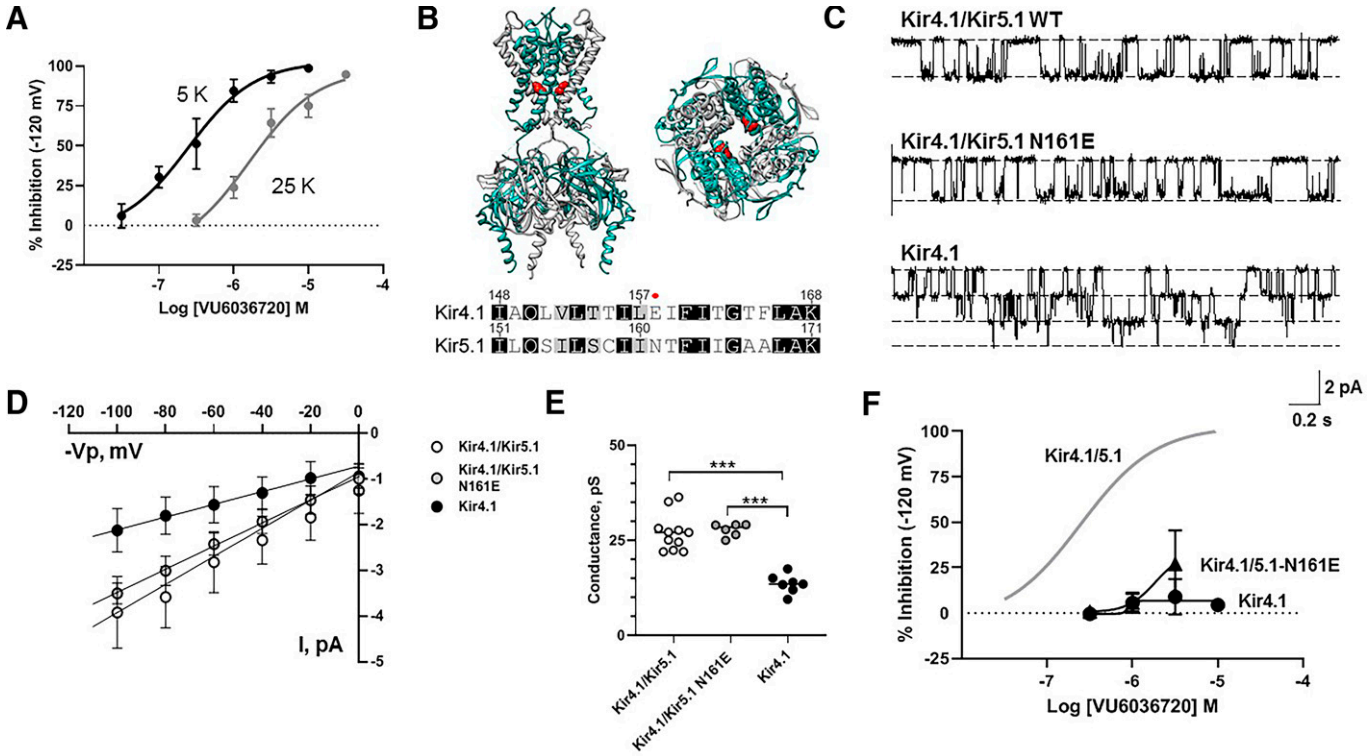

Fig. 7. VU6036720 is an inward rectifier potassium (Kir) 4.1/5.1 channel pore blocker. (A) VU6036720 CRC generated in the presence of 5 mM of potassium ion (K^+) (IC_{50} = 240 nM; black symbols and line) and 25 mM of K^+ (IC_{50} = 1.6 μM; gray symbols and line), illustrating the rightward shift associated with weakened channel block due to knockoff of VU6036720 from the intracellular pore. (B) Location of N161 in a structural model of heteromeric Kir4.1/5.1 channels based on Kir2.2 (PDB 3JYC) crystal structure. The model is shown from the side (left) and top-down (right) views in a Kir4.1-Kir5.1-Kir4.1-Kir5.1 arrangement. Kir4.1 and Kir5.1 subunits are colored gray and cyan, respectively. Alignment of Kir4.1 and Kir5.1 are shown below with a red dot indicating the location of Kir4.1-E158 and Kir5.1-N161. (C) Representative single-channel recordings of wild-type Kir4.1/5.1, Kir4.1/5.1-N161E, and Kir4.1. (D) Mean ± SD IV relationships for type Kir4.1/5.1, Kir4.1/5.1-N161, and Kir4.1. (n = 6-11). (E) Scatter plot summary showing the unitary conductances of wild-type Kir4.1/5.1 and Kir4.1/5.1-N161E are not statistically different from each other but are significantly (***$P < 0.001$) larger than that of homomeric Kir4.1. (F) Mean ± SD (n = 4-8) VU6036720 concentration-response curve for wild-type Kir4.1/Kir5.1, Kir4.1/5.1-N161E, and Kir4.1 showing dramatic effect of Kir5.1-N161E mutation on VU6036720 and essentially no activity toward Kir4.1.

TABLE 2
Pharmacokinetic parameters for VU6036720

Dose	Route	CLp (mL/min/kg)	$t_{1/2}$ (hr)	Vss (L/kg)	AUC (hr*ng/ml)
1 mg/kg	IV	124	0.68	6.00	129
Dose	Route	C_{max} (ng/ml)	t_{max} (h)	AUC (hr*ng/ml)	F (%)
10 mg/kg	PO	3.25	0.75	BLQ	NA
100 mg/kg	PO	142	0.42	207	1.30

CLp, plasma clearance; Cmax, maximal concentration; F, oral bioavailability; PO, per os (oral administration); Tmax, time of maximal concentration; Vss, volume of distribution at steady state.

fluoxetine and amitriptyline. Electrophysiological recordings showed the characteristically larger unitary conductance of Kir4.1/5.1 compared with Kir4.1. Thus, most of the channels expressed in HEK-293–Kir4.1/5.1 cells are heterotetramers.

VU6036720 is a pore blocker that likely accesses its binding site by first crossing the plasma membrane and then entering the cytoplasmic pore of the channel. Three lines of evidence support this model. First, the potency of block of inward current is reduced by increasing extracellular K^+ concentration, a phenomenon known as "knockoff" and reflects the displacement of VU6036720 from its binding site by inwardly directed K^+ ions. This behavior has been observed for small-molecule inhibitors of Kir1.1 (Lewis et al., 2009; Bhave et al., 2011), Kir2.1 (Wang et al., 2011), Kir4.1 (Kharade et al., 2018), and Kir7.1 (Swale et al., 2016). Second, bath applied VU6036720 blocks the channel in the cell-attached configuration of the patch clamp technique, making it unlikely that the compound accesses the extracellular pore of the channels being recorded. Single-channel measurements revealed that VU6036720 reduces the number of active channels, channel open probability, and unitary current amplitude. The latter effect is probably due to membrane depolarization associated with Kir4.1/5.1 channel inhibition and a reduction in the electrochemical driving force acting on K^+ ions. The third piece of evidence is that mutation of Kir5.1-N161E almost completely abrogates block of the heteromeric channel by VU6036720. This residue is located just below (intracellularly) the narrow selectivity filter of the channel, which likely creates a physical barrier between extracellular VU6036720 and its deeper binding site in the pore. The most likely explanation is that VU6036720 enters the cytoplasmic pore of the channel to reach its binding site near N161.

The development of an in vivo–active probe of Kir4.1/5.1 will be required to rigorously explore the channel's therapeutic potential as a diuretic target. Both genetic and physiologic studies support Kir4.1/5.1 as a viable diuretic target. In the DCT, Kir4.1/5.1 channels critically regulate sodium chloride reabsorption mediated by the electroneutral transporter, sodium-chloride symporter (NCC), whose activity is modulated by its phosphorylation state. Several elegant genetic, biochemical, and physiologic studies have established that the phosphorylation state of NCC is controlled by a Kir4.1/5.1-with no lysine kinase-SPS1-related proline/alanine-rich kinase -NCC regulatory pathway by which Kir4.1/5.1 channel activity promotes the phosphorylation and activity of NCC (Terker et al., 2015; Cuevas et al., 2017; Su et al., 2019; Su et al., 2020;). Genetic disruption of *KCNJ10* or depolarization of the DCT membrane potential with high K^+ decreases NCC phosphorylation/activity and reduces sodium chloride reabsorption in the DCT. Sodium that is not reabsorbed in the DCT is delivered to the cortical collecting duct where it can be reabsorbed by epithelial sodium channels, ENaC, in exchange for K^+ secretion via Kir1.1. Thus, loss of Kir4.1/5.1 in the DCT accounts for most of the sodium and K^+ wasting observed in patients with epilepsy, ataxia, sensorineural deafness, tubulopathy/seizures, sensorineural deafness, ataxia, mental disability, tubulopathy syndrome. This human genetic data offers strong validation for Kir4.1/5.1 as a novel diuretic target. The therapeutic value of Kir4.1/5.1 might be especially high in the setting of loop diuretic resistance, where the efficacy of loop diuretics is lost due in part to the expansion of the DCT and sodium chloride reabsorption capacity of this nephron segment.

We recently reported that the Kir4.1-preferring inhibitor VU0134992 induces urine volume, sodium, and K^+ wasting in orally dosed, volume-loaded rats (Kharade et al., 2018). While we intended to specifically target homomeric Kir4.1 channels expressed in the nephron, the observed diuretic effect could potentially be mediated at least in part through inhibition of Kir4.1/5.1 channels in the DCT. VU0134992 is only ninefold selective for Kir4.1 over Kir4.1/5.1 channels and diuretic effects were only observed at relatively high doses of 50 and 100 mg/kg, raising the possibility that off-target inhibition of Kir4.1/5.1 occurred. The development of an inhibitor that is highly selective for Kir4.1/5.1 over Kir4.1 is needed to test if selective inhibition of Kir4.1/5.1 is enough to induce salt and water wasting. VU6036720 is greater than 40-fold selective for Kir4.1/5.1 showing proof-of-concept that the development of highly selective probes is feasible. Unfortunately, VU6036720 showed no diuretic effects in mice, likely due to high clearance and poor bioavailability after parenteral administration. Additional chemistry is underway to identify VU6036720 analogs that maintain potency at Kir4.1/5.1 but exhibit more favorable in vivo DMPK properties.

The 4-hour dosing regimen used here should be long enough to induce a measurable diuretic response following inhibition of Kir4.1/5.1. The control diuretic used in the present study was the NCC inhibitor, HCTZ, which mediates sodium chloride reabsorption in the DCT, the same tubule segment we are targeting with a Kir4.1/5.1 inhibitor. We observed a statistically significant increase in urine volume in mice treated with HCTZ over 4 hours, but not in animals treated with VU6036720. A potentially important difference in determining the kinetics of diuresis caused by inhibiting NCC directly with HCTZ versus indirectly with an inhibitor of Kir4.1/5.1 is that the latter is mediated by the with no lysine kinase-SPS1-related proline/alanine-rich kinase SPAK-NCC pathway, which may take longer. However, several lines of evidence suggest that this should take on the order of minutes as opposed to hours or days. For example, Loffing et al. (Sorensen et al., 2013) showed that an oral K^+ load leads to rapid NCC phosphorylation and natriuresis within

30 minutes of dosing in mice. Similarly, NCC dephosphorylation is observed in kidney slices treated with high K^+ or a high dose (5 mM) of the non-specific Kir channel blocker barium (Penton et al., 2016). Taken together, these studies suggest that inhibition of Kir4.1/5.1 should trigger rapid NCC dephosphorylation and inhibition and natriuresis in vivo. The development of a potent and selective VU6036720 analog with improved DMPK properties that can effectively engage Kir4.1/5.1 in vivo will help resolve this issue.

In conclusion, we developed a robust HTS assay that enables the interrogation of large compound libraries for small-molecule modulators of heterotetrameric Kir4.1/5.1 K^+ channels. Hundreds of novel inhibitors were discovered from a screen of 80,475 chemically diverse compounds, some of which are more potent than VU6036720 even before chemical optimization (data not shown). Although VU6036720 did not exhibit in vivo activity in the metabolic cage studies reported here, it should still be useful as a selective probe of Kir4.1/5.1 function in heterologous expression experiments, isolated tubule studies, and kidney slice preparations. A surprising outcome of the primary screen is the discovery of the first-in-class potentiators of Kir4.1/5.1, which could be useful for determining how activation of the channel affects the physiology of the kidney tubule and brain astrocytes and glial cells. We anticipate that the diverse collection of chemically tractable inhibitors and activators discovered in the screen will be instrumental in transforming the molecular pharmacology of Kir4.1/5.1 by enabling the development of potent, specific, and in vivo–active channel probes.

Authorship Contributions

Participated in research design: McClenahan, Kent, Kharade, Isaeva, Williams, Han, Terker, Gresham, Lazarenko, Days, Romain, Boutaud, Sulikowski, Harris, Weaver, Staruschenko, Lindsley, Denton.

Conducted experiments: McClenahan, Kent, Kharade, Isaeva, Williams, Han, Terker, Gresham, Lazarenko, Days, Romain, Boutaud.

Performed data analysis: McClenahan, Kent, Kharade, Isaeva, Williams, Han, Terker, Gresham, Lazarenko, Days, Romain, Boutaud,

Wrote or contributed to the writing of the manuscript: McClenahan, Kent, Kharade, Isaeva, Williams, Han, Terker, Gresham, Lazarenko, Days, Romain, Boutaud, Sulikowski, Bauer, Harris, Weaver, Staruschenko, Lindsley, Denton.

References

Aréchiga-Figueroa IA, Marmolejo-Murillo LG, Cui M, Delgado-Ramírez M, van der Heyden MAG, Sánchez-Chapula JA, and Rodríguez-Menchaca AA (2017) High-potency block of Kir4.1 channels by pentamidine: Molecular basis. *Eur J Pharmacol* **815**:56–63.

Bhave G, Chauder BA, Liu W, Dawson ES, Kadakia R, Nguyen TT, Lewis LM, Meiler J, Weaver CD, Satlin LM, et al. (2011) Development of a selective small-molecule inhibitor of Kir1.1, the renal outer medullary potassium channel. *Mol Pharmacol* **79**:42–50.

Bockenhauer D, Feather S, Stanescu HC, Bandulik S, Zdebik AA, Reichold M, Tobin J, Lieberer E, Sterner C, Landoure G, et al. (2009) Epilepsy, ataxia, sensorineural deafness, tubulopathy, and KCNJ10 mutations. *N Engl J Med* **360**:1960–1970.

Bridges TM, Morrison RD, Byers FW, Luo S, and Scott Daniels J (2014) Use of a novel rapid and resource-efficient cassette dosing approach to determine the pharmacokinetics and CNS distribution of small molecule 7-transmembrane receptor allosteric modulators in rat. *Pharmacol Res Perspect* **2**:e00077.

Cuevas CA, Su XT, Wang MX, Terker AS, Lin DH, McCormick JA, Yang CL, Ellison DH, and Wang WH (2017) Potassium sensing by renal distal tubules requires Kir4.1. *J Am Soc Nephrol* **28**:1814–1825.

Cui Y, Yang Y, Ni Z, Dong Y, Cai G, Foncelle A, Ma S, Sang K, Tang S, Li Y, et al. (2018) Astroglial Kir4.1 in the lateral habenula drives neuronal bursts in depression. *Nature* **554**:323–327.

Denton JS, Pao AC, and Maduke M (2013) Novel diuretic targets. *Am J Physiol Renal Physiol* **305**:F931–F942.

Djukic B, Casper KB, Philpot BD, Chin LS, and McCarthy KD (2007) Conditional knock-out of Kir4.1 leads to glial membrane depolarization, inhibition of potassium and glutamate uptake, and enhanced short-term synaptic potentiation. *J Neurosci* **27**:11354–11365.

Dutter BF, Ender A, Sulikowski GA, and Weaver CD (2018) Rhodol-based thallium sensors for cellular imaging of potassium channel activity. *Org Biomol Chem* **16**:5575–5579.

Frizzo ME and Ohno Y (2021) Perisynaptic astrocytes as a potential target for novel antidepressant drugs. *J Pharmacol Sci* **145**:60–68.

Furutani K, Ohno Y, Inanobe A, Hibino H, and Kurachi Y (2009) Mutational and in silico analyses for antidepressant block of astroglial inward-rectifier Kir4.1 channel. *Mol Pharmacol* **75**:1287–1295.

Hibino H, Inanobe A, Furutani K, Murakami S, Findlay I, and Kurachi Y (2010) Inwardly rectifying potassium channels: their structure, function, and physiological roles. *Physiol Rev* **90**:291–366.

Jiang R, Diaz-Castro B, Looger LL, and Khakh BS (2016) Dysfunctional calcium and glutamate signaling in striatal astrocytes from Huntington's Disease model mice. *J Neurosci* **36**:3453–3470.

Kahanovitch U, Cuddapah VA, Pacheco NL, Holt LM, Mulkey DK, Percy AK, and Olsen ML (2018) MeCP2 deficiency leads to loss of glial Kir4.1. *eNeuro* **5**:ENEURO.0194-17.2018.

Kaufmann K, Romaine I, Days E, Pascual C, Malik A, Yang L, Zou B, Du Y, Sliwoski G, Morrison RD, et al. (2013) ML297 (VU0456810), the first potent and selective activator of the GIRK potassium channel, displays antiepileptic properties in mice. *ACS Chem Neurosci* **4**:1278–1286.

Kharade SV, Kurata H, Bender AM, Blobaum AL, Figueroa EE, Duran A, Kramer M, Days E, Vinson P, Flores D, et al. (2018) Discovery, characterization, and effects on renal fluid and electrolyte excretion of the Kir4.1 potassium channel pore blocker, VU0134992. *Mol Pharmacol* **94**:926–937.

Kofuji P, Biedermann B, Siddharthan V, Raap M, Iandiev I, Milenkovic I, Thomzig A, Veh RW, Bringmann A, and Reichenbach A (2002) Kir potassium channel subunit expression in retinal glial cells: implications for spatial potassium buffering. *Glia* **39**:292–303.

Lagrutta AA, Bond CT, Xia XM, Pessia M, Tucker S, and Adelman JP (1996) Inward rectifier potassium channels. Cloning, expression and structure-function studies. *Jpn Heart J* **37**:651–660.

Lewis LM, Bhave G, Chauder BA, Banerjee S, Lornsen KA, Redha R, Fallen K, Lindsley CW, Weaver CD, and Denton JS (2009) High-throughput screening reveals a small-molecule inhibitor of the renal outer medullary potassium channel and Kir7.1. *Mol Pharmacol* **76**:1094–1103.

Lin JH, Chiba M, Balani SK, Chen IW, Kwei GY, Vastag KJ, and Nishime JA (1996) Species differences in the pharmacokinetics and metabolism of indinavir, a potent human immunodeficiency virus protease inhibitor. *Drug Metab Dispos* **24**:1111–1120.

Manis AD, Hodges MR, Staruschenko A, and Palygin O (2020) Expression, localization, and functional properties of inwardly rectifying K^+ channels in the kidney. *Am J Physiol Renal Physiol* **318**:F332–F337.

Marmolejo-Murillo LG, Aréchiga-Figueroa IA, Cui M, Moreno-Galindo EG, Navarro-Polanco RA, Sánchez-Chapula JA, Ferrer T, and Rodríguez-Menchaca AA (2017a) Inhibition of Kir4.1 potassium channels by quinacrine. *Brain Res* **1663**:87–94.

Marmolejo-Murillo LG, Aréchiga-Figueroa IA, Moreno-Galindo EG, Navarro-Polanco RA, Rodríguez-Menchaca AA, Cui M, Sánchez-Chapula JA, and Ferrer T (2017b) Chloroquine blocks the Kir4.1 channels by an open-pore blocking mechanism. *Eur J Pharmacol* **800**:40–47.

Milton M and Smith PD (2018) It's all about timing: The involvement of Kir4.1 channel regulation in acute ischemic stroke pathology. *Front Cell Neurosci* **12**:36.

Nichols CG (2006) KATP channels as molecular sensors of cellular metabolism. *Nature* **440**:470–476.

Nwaobi SE, Cuddapah VA, Patterson KC, Randolph AC, and Olsen ML (2016) The role of glial-specific Kir4.1 in normal and pathological states of the CNS. *Acta Neuropathol* **132**:1–21.

Ohno Y, Hibino H, Lossin C, Inanobe A, and Kurachi Y (2007) Inhibition of astroglial Kir4.1 channels by selective serotonin reuptake inhibitors. *Brain Res* **1178**:44–51.

Penton D, Czogalla J, Wengi A, Himmerkus N, Loffing-Cueni D, Carrel M, Rajaram RD, Staub O, Bleich M, Schweda F, et al. (2016) Extracellular K^+ rapidly controls NaCl cotransporter phosphorylation in the native distal convoluted tubule by Cl^--dependent and independent mechanisms. *J Physiol* **594**:6319–6331.

Pessia M, Imbrici P, D'Adamo MC, Salvatore L, and Tucker SJ (2001) Differential pH sensitivity of Kir4.1 and Kir4.2 potassium channels and their modulation by heteropolymerisation with Kir5.1. *J Physiol* **532**:359–367.

Pessia M, Tucker SJ, Lee K, Bond CT, and Adelman JP (1996) Subunit positional effects revealed by novel heteromeric inwardly rectifying K+ channels. *EMBO J* **15**:2980–2987.

Raphemot R, Kadakia RJ, Olsen ML, Banerjee S, Days E, Smith SS, Weaver CD, and Denton JS (2013) Development and validation of fluorescence-based and automated patch clamp-based functional assays for the inward rectifier potassium channel Kir4.1. *Assay Drug Dev Technol* **11**:532–543.

Raphemot R, Lonergan DF, Nguyen TT, Utley T, Lewis LM, Kadakia R, Weaver CD, Gogliotti R, Hopkins C, Lindsley CW, et al. (2011) Discovery, characterization, and structure-activity relationships of an inhibitor of inward rectifier potassium (Kir) channels with preference for Kir2.3, Kir3.x, and Kir7.1. *Front Pharmacol* **2**:75.

Raphemot R, Swale DR, Dadi PK, Jacobson DA, Cooper P, Wojtovich AP, Banerjee S, Nichols CG, and Denton JS (2014) Direct activation of β-cell KATP channels with a novel xanthine derivative. *Mol Pharmacol* **85**:858–865.

Reichold M, Zdebik AA, Lieberer E, Rapedius M, Schmidt K, Bandulik S, Sterner C, Tegtmeier I, Penton D, Baukrowitz T, et al. (2010) KCNJ10 gene mutations causing EAST syndrome (epilepsy, ataxia, sensorineural deafness, and tubulopathy) disrupt channel function. *Proc Natl Acad Sci USA* **107**:14490–14495.

Schlingmann KP, Renigunta A, Hoorn EJ, Forst AL, Renigunta V, Atanasov V, Mahendran S, Barakat TS, Gillion V, Godefroid N, et al. (2021) Defects in KCNJ16 cause a novel tubulopathy with hypokalemia, salt wasting, disturbed acid-base homeostasis, and sensorineural deafness. *J Am Soc Nephrol* **32**:1498–1512.

Scholl UI, Choi M, Liu T, Ramaekers VT, Häusler MG, Grimmer J, Tobe SW, Farhi A, Nelson-Williams C, and Lifton RP (2009) Seizures, sensorineural deafness, ataxia,

mental retardation, and electrolyte imbalance (SeSAME syndrome) caused by mutations in KCNJ10. *Proc Natl Acad Sci USA* **106**:5842–5847.
Sorensen MV, Grossmann S, Roesinger M, Gresko N, Todkar AP, Barmettler G, Ziegler U, Odermatt A, Loffing-Cueni D, and Loffing J (2013) Rapid dephosphorylation of the renal sodium chloride cotransporter in response to oral potassium intake in mice. *Kidney Int* **83**:811–824.
Su S, Ohno Y, Lossin C, Hibino H, Inanobe A, and Kurachi Y (2007) Inhibition of astroglial inwardly rectifying Kir4.1 channels by a tricyclic antidepressant, nortriptyline. *J Pharmacol Exp Ther* **320**:573–580.
Su XT, Ellison DH, and Wang WH (2019) Kir4.1/Kir5.1 in the DCT plays a role in the regulation of renal K^+ excretion. *Am J Physiol Renal Physiol* **316**:F582–F586.
Su XT, Klett NJ, Sharma A, Allen CN, Wang WH, Yang CL, and Ellison DH (2020) Distal convoluted tubule Cl^- concentration is modulated via K^+ channels and transporters. *Am J Physiol Renal Physiol* **319**:F534–F540.
Su XT and Wang WH (2016) The expression, regulation, and function of Kir4.1 (Kcnj10) in the mammalian kidney. *Am J Physiol Renal Physiol* **311**:F12–F15.
Swale DR, Kharade SV, and Denton JS (2014) Cardiac and renal inward rectifier potassium channel pharmacology: emerging tools for integrative physiology and therapeutics. *Curr Opin Pharmacol* **15**:7–15.
Swale DR, Kurata H, Kharade SV, Sheehan J, Raphemot R, Voigtritter KR, Figueroa EE, Meiler J, Blobaum AL, Lindsley CW, et al. (2016) ML418: The first selective, sub-micromolar pore blocker of Kir7.1 potassium channels. *ACS Chem Neurosci* **7**:1013–1023.
Terker AS, Zhang C, McCormick JA, Lazelle RA, Zhang C, Meermeier NP, Siler DA, Park HJ, Fu Y, Cohen DM, et al. (2015) Potassium modulates electrolyte balance and blood pressure through effects on distal cell voltage and chloride. *Cell Metab* **21**:39–50.
Tong X, Ao Y, Faas GC, Nwaobi SE, Xu J, Haustein MD, Anderson MA, Mody I, Olsen ML, Sofroniew MV, et al. (2014) Astrocyte Kir4.1 ion channel deficits contribute to neuronal dysfunction in Huntington's disease model mice. *Nat Neurosci* **17**:694–703.
Tucker SJ, Imbrici P, Salvatore L, D'Adamo MC, and Pessia M (2000) pH dependence of the inwardly rectifying potassium channel, Kir5.1, and localization in renal tubular epithelia. *J Biol Chem* **275**:16404–16407.
Wang HR, Wu M, Yu H, Long S, Stevens A, Engers DW, Sackin H, Daniels JS, Dawson ES, Hopkins CR, et al. (2011) Selective inhibition of the K(ir)2 family of inward rectifier potassium channels by a small molecule probe: the discovery, SAR, and pharmacological characterization of ML133. *ACS Chem Biol* **6**:845–856.
Weaver CD and Denton JS (2021) Next-generation inward rectifier potassium channel modulators: discovery and molecular pharmacology. *Am J Physiol Cell Physiol* **320**:C1125–C1140.
Webb BD, Hotchkiss H, Prasun P, Gelb BD, and Satlin L (2021) Biallelic loss-of-function variants in KCNJ16 presenting with hypokalemic metabolic acidosis. *Eur J Hum Genet* **29**:1566–1569.
Welling PA (2016) Roles and Regulation of Renal K Channels. *Annu Rev Physiol* **78**:415–435.
Zhang C, Wang L, Zhang J, Su XT, Lin DH, Scholl UI, Giebisch G, Lifton RP, and Wang WH (2014) KCNJ10 determines the expression of the apical Na-Cl cotransporter (NCC) in the early distal convoluted tubule (DCT1). *Proc Natl Acad Sci USA* **111**:11864–11869.
Zhang X, Su J, Cui N, Gai H, Wu Z, and Jiang C (2011) The disruption of central CO2 chemosensitivity in a mouse model of Rett syndrome. *Am J Physiol Cell Physiol* **301**:C729–C738.

Address correspondence to: Dr. Jerod S. Denton, 1161 21st Avenue South, T4208 Medical Center North, Nashville, TN 37232. E-mail: jerod.s.denton@vumc.org